

|             |  |
|-------------|--|
| Title       | Self-assembling nano-probes displaying off/on $^{19}\text{F}$ NMR signals for protein detection and imaging                                      |
| Author(s)   | Takaoka, Yousuke; Sakamoto, Takashi; Tsukiji, Shinya; Narazaki, Michiko; Matsuda, Tetsuya; Tochio, Hidehito; Shirakawa, Masahiro; Hamachi, Itaru |
| Citation    | Nature Chemistry (2009), 1(7): 557-561   |
| Issue Date  | 2009-10  |
| URL         | <a href="http://hdl.handle.net/2433/85342">http://hdl.handle.net/2433/85342</a>  |
| Right       | c 2009 Nature Publishing Group. 許諾条件により本文は2010-03-24に公開.   |
| Type        | Journal Article  |
| Textversion | author   |

5  
6 **Self-assembling nano-probes displaying off/on  $^{19}\text{F}$  NMR signal**  
7 **for protein detection and imaging**  
8

9 Yousuke Takaoka,<sup>1</sup> Takashi Sakamoto,<sup>1</sup> Shinya Tsukiji,<sup>1,4</sup> Michiko Narazaki,<sup>2</sup> Tetsuya  
10 Matsuda,<sup>2</sup> Hidehito Tochio,<sup>3</sup> Masahiro Shirakawa<sup>3</sup> & Itaru Hamachi<sup>1,4</sup>

11  
12 <sup>1</sup>Department of Synthetic Chemistry and Biological Chemistry, Graduate School of  
13 Engineering, Kyoto University, Katsura, Nishikyo-ku, Kyoto 615-8510, JAPAN

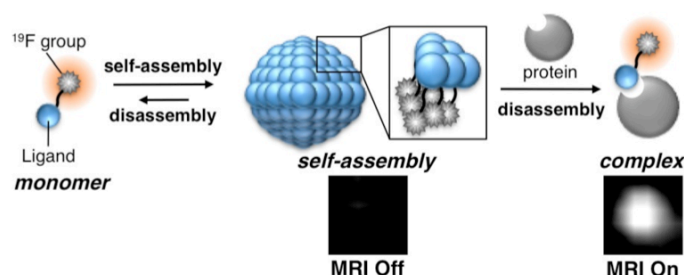
14 <sup>2</sup>Department of Systems Science, Graduate School of Informatics, Kyoto University,  
15 36-1 Yoshida-Honmachi, Sakyo-ku, Kyoto 606-8501, JAPAN

16 <sup>3</sup>Department of Molecular Engineering, Graduate School of Engineering, Kyoto  
17 University, Katsura, Nishikyo-ku, Kyoto 615-8510, JAPAN

18 <sup>4</sup>CREST(Core Research for Evolutional Science and Technology, JST), Sanbancho,  
19 Chiyodaku, Tokyo, 102-0075, JAPAN

20 Correspondence should be addressed to I.H. (ihamachi@sbchem.kyoto-u.ac.jp).

21  
22  
23 **TABLE OF CONTENTS (90 mm x 40 mm)**  
24



1 **ABSTRACT (150 words)**

2 **Magnetic resonance imaging (MRI) is one of the most promising techniques for**  
3 **non-invasive visualization of biomarkers and biologically relevant species both in**  
4 **vivo and ex vivo. Although  $^1\text{H}$  MRI with paramagnetic contrast agents, such as**  
5  **$\text{Gd}^{3+}$  complexes and iron oxide, is widely used, it often suffers from low contrast**  
6 **due to the large background signals from the abundant distribution of protons in**  
7 **biological samples. Here we report supramolecular organic nanoparticles to detect**  
8 **specific proteins by  $^{19}\text{F}$ -based MRI in a perfect off/on mode. The designed probes**  
9 **are NMR-silent when aggregated but, in the presence of a target protein, are**  
10 **disassembled to produce a sharp signal. This "turn-on" response allowed us to**  
11 **clearly visualize the proteins inside live cells by  $^{19}\text{F}$  MRI and construct an in-cell**  
12 **inhibitor assay. This recognition-driven disassembly of nano-probes for turn-on**  
13  **$^{19}\text{F}$ -signal is unprecedented and this strategy may extend the utility of  $^{19}\text{F}$  MRI for**  
14 **specific protein imaging. (150 words)**

15  
16  
17 **MAIN TEXT (2,000 words)**

18 MRI is superior to optical bio-imaging in living systems for the visualization of  
19 deep tissues.<sup>1-3</sup> Currently,  $^1\text{H}$  MRI is widely used for diagnostic purposes because of its  
20 high sensitivity. This high sensitivity is attributed to the abundance of water molecules  
21 in the vicinity of contrast agents. However, at the same time,  $^1\text{H}$  MRI often suffers from  
22 low contrast-to-noise ratio due to the large background signals from water protons.  
23 Therefore, for specific imaging of biomarkers and biologically relevant molecules with  
24 higher functional and/or spatial resolution in vivo as well as ex vivo, there is still an  
25 obvious need to develop new methodologies. Several approaches are now proposed.<sup>2-6</sup>  
26 In particular,  $^{19}\text{F}$  holds great promise as an alternative nuclide for MRI as it has a high  
27 NMR sensitivity next to  $^1\text{H}$  (83% relative to  $^1\text{H}$ ) and 100% natural abundance. A more  
28 important advantage of  $^{19}\text{F}$  is that essentially no NMR-detectable  $^{19}\text{F}$  is present in  
29 animal bodies, eliminating the interference from background signals.<sup>7,8</sup> As such, when a  
30  $^{19}\text{F}$ -containing probe is applied to a biological sample, only the extrinsic signal from the  
31 molecule can be detected. However,  $^{19}\text{F}$  MRI technology is still in its infancy. Despite  
32 significant importance for medical diagnosis, strategies for imaging specific  
33 proteins/enzymes with high MRI contrast are very limited. To date, targeting or

1 switching probes for  $^{19}\text{F}$  NMR/MRI detection have been proposed. The former is based  
2 on the accumulation of probes in specific regions in tissues through binding to localized  
3 components,<sup>9</sup> while the latter provides signals that can be modulated by enzymatic  
4 reaction. Two types of switching  $^{19}\text{F}$  MRI probes reported were enzyme substrates: one  
5 displays chemical shift changes<sup>10</sup> and the other shows a paramagnetic relaxation  
6 enhancement (PRE)-dependent signal turn-on, upon enzymatic cleavages.<sup>11</sup> The  
7 switching of these probes relies entirely on the catalytic activity of the enzymes, and  
8 thus the probes are spatially diffused away from the target enzyme and also not  
9 applicable for non-enzymatic protein targets. Therefore, more universal MRI strategies  
10 for protein detection and imaging that do not rely on enzymatic activities are highly  
11 desirable.

12 Here we describe a novel strategy to detect specific proteins with an ‘off/on-type’  
13  $^{19}\text{F}$  NMR signal using dynamic self-assembled nano-particles. Our idea is based on that  
14 the  $^{19}\text{F}$  NMR signal is broadened and attenuated when the molecules assemble into  
15 high-molecular weight aggregates, but recovers upon their disassembly.<sup>2</sup> Because  $^{19}\text{F}$   
16 has a relatively large chemical shift anisotropy (CSA; approximately 39 ppm for  $-\text{CF}_3$   
17 group),<sup>12</sup> the transverse relaxation of  $^{19}\text{F}$  NMR signals is extremely sensitive to the  
18 apparent molecular weight, due to the CSA relaxation mechanism. Thus, formation of a  
19 large molecular assembly can cause severe broadening of the  $^{19}\text{F}$  NMR signal.  
20 Accordingly, small molecule probes were designed which are composed of a  
21  $^{19}\text{F}$ -containing group and a ligand specific to a protein of interest, and concurrently  
22 equipped with the ability to form nano-aggregates. The probe alone is NMR-silent due  
23 to its self-assembly, but gives a distinct  $^{19}\text{F}$  signal in response to the target protein  
24 through the binding-mediated disassembly of the probe (**Fig. 1a**). Since the signal  
25 response is determined by specific protein-ligand interactions, this principle should be  
26 applicable to detect the presence of certain proteins including both enzymes and  
27 non-enzymatic proteins.

28 For the proof-of-principle experiment, we initially chose human carbonic anhydrase  
29 I (hCAI) as a target protein. Probe **1** was synthesized which contains a  
30 3,5-bis(trifluoromethyl)benzene (FB) derivative carrying six magnetically equivalent  
31  $^{19}\text{F}$  nuclei connected to a benzenesulfonamide moiety, a ligand specific for hCAI  
32 (dissociation constant  $K_d = \text{ca. } 3 \mu\text{M}$ ),<sup>13</sup> via a relatively hydrophobic linker (**Fig. 1b** and  
33 **Supplementary Methods**). When **1** was dissolved in a buffer solution containing

1 trifluoroacetic acid (TFA; internal standard at -75.6 ppm), no  $^{19}\text{F}$  signal was observed.  
2 However, a sharp signal appeared at -62.6 ppm upon addition of hCAI (**Fig. 1d**). The  
3 signal intensity increased linearly in proportional to the concentration of hCAI, and was  
4 saturated at a 1:1 molar ratio of probe **1** and hCAI (**Fig. 1e**). By the subsequent addition  
5 of a strong inhibitor, EZA (ethoxzolamide, **2**; **Fig. 1c**),<sup>14</sup> into the above solution, the  
6 signal disappeared again (**Supplementary Fig. 1a**). These data indicate that 1) probe **1**  
7 alone is NMR silent, 2) the appeared  $^{19}\text{F}$  signal can be assigned to the probe **1** bound to  
8 the ligand-binding pocket of hCAI, and 3) the signal can be turned off in a reversible  
9 manner when the probe is expelled from the protein (that is, when the target protein is  
10 incapable of binding the probe). We next examined the target-specificity of probe **1**  
11 under miscellaneous conditions. Addition of **1** to a mixture of four proteins different  
12 from hCAI (hemoglobin, bovine serum albumin, concanavaline A, and chymotrypsin)  
13 did not give any sharp signal. On the other hand, the  $^{19}\text{F}$  signal was clearly observed in a  
14 mixture containing the four proteins and hCAI (**Supplementary Fig. 1c**). We also found  
15 that the hCAI-induced appearance of the  $^{19}\text{F}$  signal took place in 70 % fetal bovine  
16 serum solution which contains many biological substances including proteins, lipids,  
17 and small molecules (**Supplementary Fig. 1d**). Overall, these results clearly  
18 demonstrate that probe **1** can selectively detect hCAI by turned-on  $^{19}\text{F}$  signal even in  
19 crude samples.

20 The self-assembly/disassembly properties of probe **1** were investigated by various  
21 measurements. Spherical or oval aggregates of **1** with a size ranging from 200 to 500  
22 nm in diameter were observed by atomic force microscopy (AFM) (**Fig. 2a**).  
23 Transmission electron microscopy (TEM) and scanning electron microscopy (SEM)  
24 data supported the formation of aggregates of approximately 200 nm in size (**Fig. 2b**  
25 **and Supplementary Fig. 2a**). The UV-visible absorption spectrum of **1** in buffer  
26 solution showed a broad visible light scattering around 500–700 nm due to the  
27 aggregates of **1** (**Fig. 2c and Supplementary Fig. 2b**). The scattering was decreased  
28 10-fold by the addition of hCAI, indicating that the aggregates were efficiently  
29 collapsed by hCAI. The aggregates with a mean size of 250 nm in diameter were  
30 consistently shown by dynamic light scattering (DLS) measurements in buffer solution  
31 containing **1** alone (**Fig. 2d**), whereas negligible DLS intensity was obtained after  
32 adding hCAI to the above solution. The molecular weight (Mw) of the nano-aggregate  
33 of **1** roughly estimated by the observed diameter is  $10^7$  Da, while the Mw of the

1 complex between hCAI and probe **1** is  $3 \times 10^4$  Da. We thus conclude that the binding of  
2 probe **1** to hCAI induces the disassembly of the nano-aggregates, which dramatically  
3 decreases the apparent Mw. This decrease effectively reduces the  $^{19}\text{F}$  relaxation rate, so  
4 that a sharp  $^{19}\text{F}$  signal can be observed. By the concentration dependence of DLS  
5 measurement, the critical aggregation concentration (CAC) of the self-assembly of **1**  
6 was revealed to be  $< 5 \mu\text{M}$  (**Supplementary Fig.2c**).

7 On the basis of this principle, we next produced a turn-on  $^{19}\text{F}$  probe **3** for trypsin  
8 (TPS). Instead of benzenesulfonamide, benzamidin, a typical inhibitor for TPS ( $K_d = \text{ca.}$   
9  $20 \mu\text{M}$ ),<sup>15</sup> was linked to the FB moiety as a suitable ligand. Almost no NMR signal was  
10 detected in buffer solution containing probe **3** alone, whereas a new signal was  
11 intensified upon addition of TPS (**Fig. 3a**). In the presence of benzamidin (**4**, **Fig. 1c**),  
12 such signal intensification did not occur. Similarly, biotin-tethered probe **5** showed a  
13 clear off/on  $^{19}\text{F}$  NMR response to a non-enzymatic protein, avidin ( $K_d$  of biotin,  $\text{ca. } 10^{-15}$   
14  $\text{M}$ )<sup>16</sup> (**Fig. 3b**). Furthermore, the orthogonality of probe **1** and **5** was investigated. It was  
15 shown that **1** responded to hCAI but not to avidin, and vice versa for **5** (**Supplementary**  
16 **Fig.3**). These data demonstrate the general applicability of the present strategy for  
17 designing turn-on supramolecular nano-probes to detect target proteins by  $^{19}\text{F}$  NMR  
18 spectroscopy.

19 Notably, probe **1** was also capable of detecting hCA within live cells. hCA is a  
20 cytosolic protein and naturally expressed inside human red blood cells (RBCs) (at a  
21 concentration of approximately  $170 \mu\text{M}$ ).<sup>17</sup> A suspension of RBCs was incubated with **1**  
22 for a few minutes, and after collecting cells, *in cell*  $^{19}\text{F}$  NMR analysis was conducted.  
23 Note that no hemolysis occurred during the experiments. A signal was clearly observed  
24 at  $-62.6 \text{ ppm}$  (**Fig. 4a**, top), with a chemical shift of which is identical to that obtained  
25 using purified hCAI and **1** (**Fig. 1d**), although there was a slight peak broadening. In  
26 contrast, no signal appeared when **1** was incubated with RBCs in the presence of EZA  
27 (**Fig. 4a**, bottom). Clearly, probe **1** is cell-permeable and can specifically detect  
28 endogenous hCA with turn-on signal response even inside cells.

29 The perfect turn-on probe **1** allowed us to visualize the target protein using a  $^{19}\text{F}$   
30 MRI phantom. At first,  $^1\text{H}$  and  $^{19}\text{F}$  MR images were acquired after mixing hCAI with  
31 probe **1** under in test tube conditions in the absence (sample 1) and presence of the  
32 inhibitor, EZA (sample 2) or SBA (4-sulfamoylbenzoic acid, **7**, **Fig. 1c**)<sup>13</sup> (sample 3). In  
33  $^1\text{H}$  MRI, all of the three samples gave indistinguishable images (**Fig. 4b**, top). On the

1 other hand, a distinct  $^{19}\text{F}$  MR image was obtained from sample 1, whereas no MRI  
2 signal was detected in sample 2 and 3 (**Fig. 4b**, bottom). These results are consistent  
3 with the  $^{19}\text{F}$  NMR data described above (**Fig. 1d** and **Supplementary Fig. 1a**). More  
4 significantly, a clear  $^{19}\text{F}$  MR image was observed in sample 4 containing RBCs and  
5 probe **1** (**Fig. 4c**). The MR image was completely diminished by co-incubation of EZA  
6 (sample 5), confirming that the positive MR image obtained above is indeed due to  
7 probe **1** bound to hCAI inside cells. Interestingly, sample 6 containing RBCs, probe **1**  
8 and SBA still gave a MR image similar to that of sample 4 despite the presence of the  
9 inhibitor. Given that the SBA efficiently blocks the binding of probe **1** to hCAI under in  
10 test tube conditions (**Fig. 4b**, bottom), this result is reasonably ascribed to the less  
11 cell-membrane permeability of anionic SBA compared to neutral EZA. Therefore, the  
12 present system serves as a cell-based inhibitor screening platform which can visualize  
13 the potency of inhibitors in cellular contexts.

14 In conclusion, we have developed the supramolecular  $^{19}\text{F}$ -containing nano-probes  
15 which can detect specific proteins spatially by the  $^{19}\text{F}$  MRI technique with sharp  
16 turn-on-type switching. The simple principle for the off/on response, i.e. self-assembly  
17 and recognition-driven disassembly of the nano-probe,<sup>18</sup> should be applicable to the  
18 design of other turn-on probes for various target proteins by appropriately replacing the  
19 ligand module, as shown in the case of TPS probe **3** and avidin probe **5**. It should also  
20 be noted that, in contrast to existing MRI contrast agents,<sup>1-6, 11</sup> this method does not  
21 require any metals that have potential toxicity. In the practical viewpoint, it may be fair  
22 to consider that the sensitivity of  $^{19}\text{F}$  is considerably low compared to  $^1\text{H}$  MRI and thus  
23 the present system is not yet sufficient for in vivo or clinical application using  
24 conventional bench-top spectrometers (which generally have strengths of  $\sim 1$  tesla).  
25 Functional  $^{19}\text{F}$  probes are also very limited in number. However, we believe that with  
26 further advances in both instrumentation and chemistry,  $^{19}\text{F}$ -based NMR/MRI technique  
27 may become a more powerful modality for practical diagnosis as well as basic research  
28 in the future. It is essential for chemists to establish general and useful design concepts  
29 for new  $^{19}\text{F}$  probes that facilitate functional and molecular MRI. (1854 words)

30

31

## 32 **METHODS (800 words)**

### 33 **$^{19}\text{F}$ NMR analysis of probe **1** with various concentrations of hCAI**

1 Human carbonic anhydrase I (hCAI, 5.0 mg) was dissolved in 50 mM HEPES  
2 buffer (1.0 mL, pH 7.2, 10% D<sub>2</sub>O (v/v), 0.2 mM TFA). The concentration of hCAI was  
3 determined by absorbance at 280 nm using the molar extinction coefficient (49 000  
4 M<sup>-1</sup>cm<sup>-1</sup>)<sup>19</sup> and 100 μM stock solution was prepared. Probe **1** (3.0 mg, 3.8 μmol) was  
5 dissolved in 75 μL of DMSO as the stock solution, and slowly added to the hCAI  
6 solution (0.6% DMSO (v/v)). These samples were analyzed by <sup>19</sup>F NMR with TFA as an  
7 internal standard (-75.6 ppm).

### 8 9 **AFM, TEM and SEM observations**

10 AFM imaging; a solution of probe **1** was spin coated onto a freshly cleaved mica  
11 surface and dried in vacuo. The sample was imaged by a tapping-mode AFM on a  
12 SEIKO SPA-400. TEM imaging; a solution of probe **1** was deposited on a thin carbon  
13 support film and dried in vacuo. The sample was imaged by a JEOL JEM-1025,  
14 operating at 100 kV, without any contrast agent. SEM imaging; a solution of probe **1**  
15 was deposited on a silicon wafer and dried in vacuo. The sample was imaged by a JEOL  
16 JFC-1600, operating at 15 kV, with the addition of platinum spray as a conductive  
17 material.

### 18 19 **Measurements of optical density and dynamic light scattering**

20 The optical density was measured at 25°C in 50 mM HEPES buffer (pH 7.2, 0.2  
21 mM TFA) using a quartz cell (1 cm). The DMSO stock solution of probe **1** was slowly  
22 added to the buffer solution (0.6% DMSO (v/v)) to be 25 μM. The measurements of  
23 dynamic light scattering were performed in the same conditions using a tubular-type cell.  
24 All measurements were performed in triplicate.

### 25 26 **<sup>19</sup>F NMR analyses of probe **3** and probe **5****

27 Trypsin (TPS, 5.0 mg) was dissolved in 50 mM Tris-HCl buffer (1.0 mL, pH 8.5,  
28 300 mM NaCl, 0.2 mM TFA, 10% D<sub>2</sub>O (v/v)). The concentration of TPS was  
29 determined by absorbance at 280 nm using the molar extinction coefficient (36 700  
30 M<sup>-1</sup>cm<sup>-1</sup>)<sup>20</sup> and 100 μM stock solution was prepared. The probe **3** (1.0 mg, 1.3 μmol)  
31 was dissolved in 26 μL of DMSO and 26 μL of 50 mM Tris-HCl buffer (pH 8.5) as the  
32 stock solution (25 mM), and slowly added to the TPS solution (0.2% DMSO (v/v)).  
33 Avidin (5.0 mg) was dissolved in 50 mM HEPES buffer (1.0 mL, pH 7.2, 500 mM NaCl,



1 0.2 mM TFA, 10% D<sub>2</sub>O (v/v)). The concentration of avidin was determined by  
2 absorbance at 280 nm using the molar extinction coefficient (35 700 M<sup>-1</sup>cm<sup>-1</sup>)<sup>21</sup> and 100  
3 μM stock solution was prepared. The probe **5** (3.0 mg, 3.8 μmol) was dissolved in 72  
4 μL of DMSO as the stock solution, and slowly added to the avidin solution (0.6%  
5 DMSO (v/v)). Conditions for <sup>19</sup>F NMR measurements were same as probe **1**.

### 7 **HCA Inhibitor assays in RBCs**

8 A 2 mL solution of probe **1** (200 μM) and inhibitor (EZA or SBA, 0 or 1 mM) in  
9 HBS buffer (20 mM HEPES, 107 mM NaCl, 6 mM KCl, 1.2 mM MgSO<sub>4</sub>, 2 mM CaCl<sub>2</sub>,  
10 11.5 mM glucose, pH 7.4) was added to 2 mL of sedimented red blood cells (RBCs),  
11 and the suspension was incubated at room temperature for a few minutes. After  
12 centrifugation (1,500 rpm × 5 min), the supernatant was removed and re-suspended in  
13 buffer for <sup>19</sup>F NMR measurement (50 mM HEPES buffer (pH 7.2), 100 mM NaCl, 0.17  
14 mM TFA, 20% D<sub>2</sub>O (v/v)). 0.7 mL and 2.5 mL of the suspension were used for <sup>19</sup>F  
15 NMR and MRI measurement at 25°C, respectively.

### 17 **<sup>1</sup>H and <sup>19</sup>F MRI in test tube or in RBCs**

18 <sup>1</sup>H images of sample 1-3 (in test tube) were obtained by gradient echo with  
19 repetition time (TR) /echo time (TE) = 100/6 ms, flip angle = 30, field of view (FOV) =  
20 16 x 4 cm, slice thickness = 5 mm, matrix size = 256 x 256 and 1 average. <sup>19</sup>F images of  
21 sample 1-3 (in test tube) were obtained by fast spin echo with TR / TE = 1500/5.5 ms,  
22 echo train length = 32, FOV = 16 x 4 cm without slice selection, matrix size = 128 x 32,  
23 the depth of sample tube was 20 mm, voxel size was approximately 31 mm<sup>3</sup>, and 1200  
24 averages. <sup>19</sup>F images of sample 4-6 (in RBCs) were obtained by gradient spin echo with  
25 TR / TE = 1000/2.4 ms, flip angle = 90, FOV = 32 x 8 cm without slice selection,  
26 matrix size = 128 x 32, the depth of sample tube was 30 mm, voxel size was  
27 approximately 188 mm<sup>3</sup>, and 400 averages. The sine window function was applied to  
28 the <sup>19</sup>F images. All the images were acquired at 25°C. (787 words)

1 **ACKNOWLEDGEMENT**

2 We thank E. Ashihara (Kyoto University Hospital) for the collection of blood  
3 samples, J. Miyake and T. Kunita (Kyoto University) for help with AFM and SEM  
4 measurements. Y.T acknowledges the JSPS Research Fellowships for Young Scientists.  
5 This work was partly supported by CK integrated Medical Bio-imaging Project  
6 (MEXT) and by CREST (JST).

7

8

9 **AUTHOR CONTRIBUTIONS**

10 I.H. conceived of the project. Y.T., T.S., S.T. and I.H. designed the experiments. Y.T.  
11 performed all the experiments, with help from H.T. and M.S. on  $^{19}\text{F}$  NMR  
12 measurements. M.N. and T.M. performed the MRI experiments. The manuscript was  
13 written by Y.T., S.T. and I.H., with editing by all the co-authors.

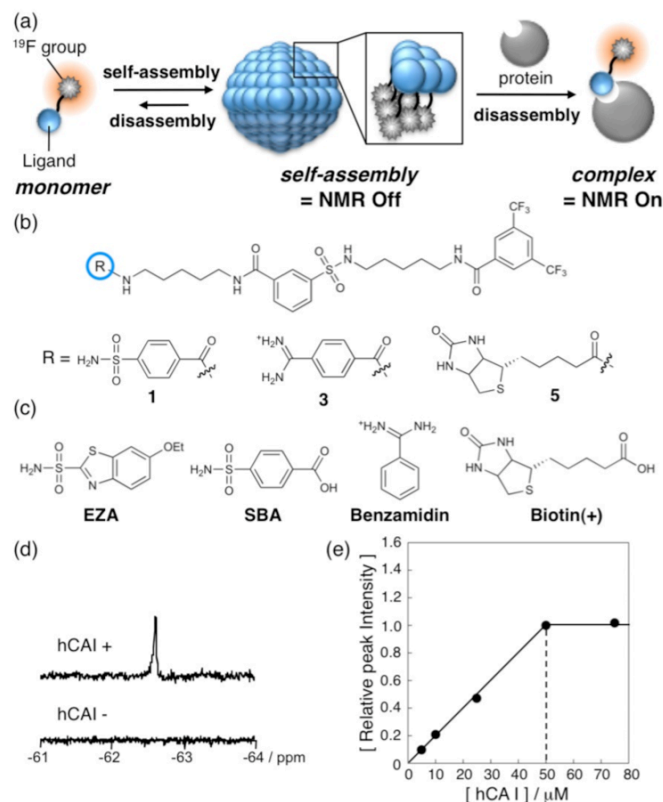
1   **REFERENCES**

- 2   1) Kiessling, F., Morgenstern, B., Zhang, C. *Curr. Med. Chem.*, **14**, 77-91 (2007).  
3   2) Perez, J. M., Josephson, L., O'Loughlin, T., Hogemann, D., Weissleder, R. *Nat.*  
4   *Biotechnol.*, **20**, 816-820 (2002).  
5   3) Louie, A. Y. *et al. Nat. Biotechnol.*, **18**, 321-325 (2000).  
6   4) Sosnovik, D. E., Weissleder, R. *Curr. Opin. Biotech.*, **18**, 4-10 (2007).  
7   5) Woods, M., Woessner, D. E., Sherry A. D. *Chem. Soc. Rev.*, **35**, 500-511 (2006).  
8   6) Jun, Y., Lee, J-H., Cheon, J. *Angew. Chem. Int. Ed.*, **47**, 5122-5135 (2008).  
9   7) Danielson, M. A. & Falke, J. J. *Annu. Rev. Biophys. Biomol. Struct.*, **25**, 163-195  
10   (1996).  
11   8) Yu, J., Kodibagkar, V. D., Cui, W., Mason, R. P. *Curr. Med. Chem.*, **12**, 819-848  
12   (2005).  
13   9) Higuchi, M. *et al. Nat. Neurosci.*, **8**, 527-533 (2005).  
14   10) Yu, J., Liu, L., Kodibagkar, V. D., Cui, W., Mason, R. P. *Bioorg. Med. Chem.*, **14**,  
15   326-333 (2006).  
16   11) Mizukami, S. *et al. J. Am. Chem. Soc.*, **130**, 794-795 (2008).  
17   12) Grage, S. L. *et al. J. Magn. Reson.*, **191**, 16-23 (2008).  
18   13) Taylor, P. W., King, R. W., Burgen, A. S. V. *Biochemistry*, **9**, 2638-2645 (1970).  
19   14) Casini, A. *et al. Bioorg. Med. Chem. Lett.*, **13**, 841-845 (2003).  
20   15) Talhout, R., Villa, A., Mark, A. E., Engberts, J. B. F. N. *J. Am. Chem. Soc.*, **125**,  
21   10570-10579 (2003).  
22   16) Green, N. M. *Biochem. J.*, **89**, 585-591 (1963).  
23   17) Casey, J. R. *et al. J. Med. Chem.*, **47**, 2337-2347 (2004).  
24   18) Savariar, E. N., Ghosh, S., González, D. C., Thayumanavan, S. *J. Am. Chem. Soc.*,  
25   **130**, 5416-5417 (2008).  
26   19) Chazalatte, C. *et al. Bioorg. Med. Chem. Lett.*, **14**, 5781-5786 (2004).  
27   20) Talhout, R., Engberts, J. B. F. N. *Eur. J. Biochem.*, **268**, 1554-1560 (2001).  
28   21) Finn, F. M., Titus, G., Montibeller, J. A., Hofmann, K. *J. Biol. Chem.*, **255**,  
29   5742-5746 (1980).

30

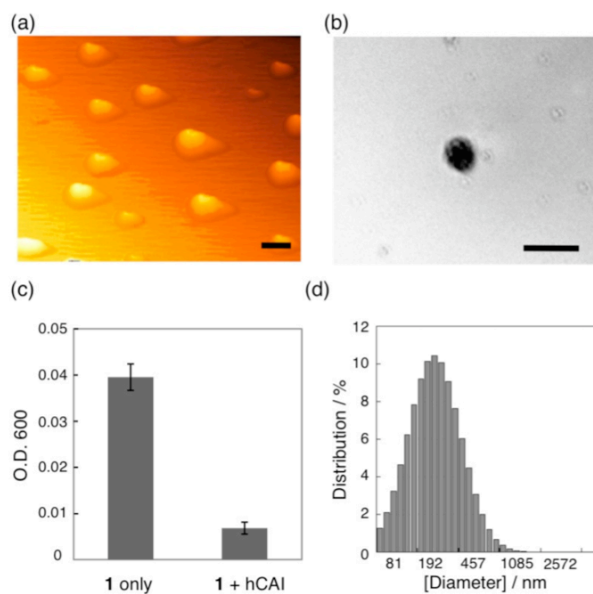
31

1 **Figures:**



2  
 3 **Figure 1.** The turn-on-type  $^{19}\text{F}$  NMR probes for protein imaging. (a) Schematic  
 4 illustration of the present strategy for an off/on switching mode of  $^{19}\text{F}$  NMR. (b)  
 5 Chemical structures of probe **1**, **3** and **5** for hCAI, TPS and avidin, respectively. (c)  
 6 Chemical structures of inhibitors. For hCAI, EZA (ethoxzolamide, **2**) and SBA  
 7 (4-sulfamoylbenzoic acid, **7**); for TPS, Benzamidin (**4**); for avidin, Biotin(+) (**6**). (d)  
 8 Turn-on  $^{19}\text{F}$  NMR signal of probe **1** (50  $\mu\text{M}$ ) in the presence (top) or absence (bottom)  
 9 of hCAI (50  $\mu\text{M}$ ). The signal to noise ratio (SNR) was 60.1. (e) Dependence of the  
 10  $^{19}\text{F}$ -signal intensity (-62.6 ppm) on the hCAI concentration: probe **1** (50  $\mu\text{M}$ ) in 50 mM  
 11 HEPES buffer (pH 7.2, 0.2 mM TFA as an internal standard for peak intensity and  
 12 chemical shift, 10% D<sub>2</sub>O (v/v)) at 25°C.

13  
 14

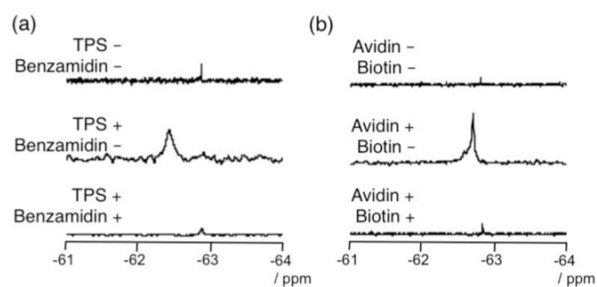


1

2 **Figure 2.** Microscopic and spectroscopic characterization of the self-assembled  
 3 nano-particles of probe **1**. **(a)** AFM image of the self-assembled probe **1** (25  $\mu$ M). The  
 4 scale bar is 500 nm. **(b)** TEM image of the self-assembled probe **1** (25  $\mu$ M). The scale  
 5 bar is 500 nm. **(c)** Optical density at 600 nm of aqueous solution containing probe **1** (25  
 6  $\mu$ M) in the absence (left) or presence (right) of hCAI (25  $\mu$ M). Experiments were  
 7 performed in triplicate to obtain mean and standard deviation values (shown as error  
 8 bars). **(d)** DLS analysis of particle size distribution of the self-assembled probe **1** (25  
 9  $\mu$ M). All experiments were performed in 50 mM HEPES buffer (pH 7.2, 0.2 mM TFA).

10

11

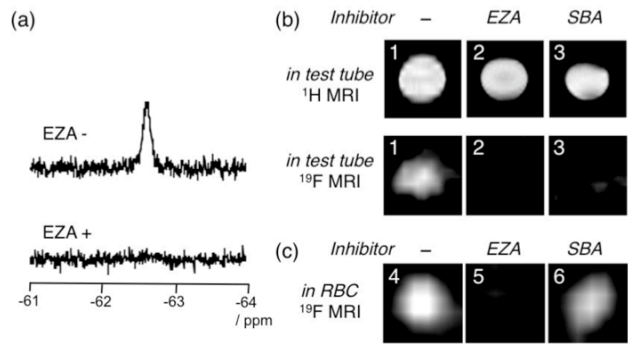


1

2 **Figure 3.** Turn-on <sup>19</sup>F NMR detection of trypsin and avidin by probe **3** and **5**. **(a)** <sup>19</sup>F  
 3 NMR spectra of **3** (100 μM) in the absence or presence of TPS (50 μM) and benzamidine  
 4 (500 μM) in 50 mM Tris-HCl buffer (pH 8.5, 0.2 mM TFA, 300 mM NaCl, 10% D<sub>2</sub>O  
 5 (v/v)). The SNR was 12.2. **(b)** <sup>19</sup>F NMR spectra of **5** (100 μM) in the absence or  
 6 presence of avidin (50 μM) and biotin (500 μM) in 50 mM HEPES buffer (pH 7.2, 0.2  
 7 mM TFA, 500 mM NaCl, 10% D<sub>2</sub>O (v/v)). The SNR was 57.3.

8

9



1  
2  
3  
4  
5  
6  
7  
8  
9  
10  
11  
12  
13

**Figure 4.**  $^{19}\text{F}$  NMR spectra and MR images in red blood cells (RBCs). **(a)**  $^{19}\text{F}$  NMR spectra of probe **1** in the absence (top) or presence (bottom) of EZA in RBCs. The SNR was 14.2. **(b)** MR images of probe **1** in test tube (top;  $^1\text{H}$ , bottom;  $^{19}\text{F}$ ). **(c)** MR images of probe **1** in RBCs. Conditions: For in test tube (sample 1-3); **1** (100  $\mu\text{M}$ ), hCAI (50  $\mu\text{M}$ ), inhibitors (EZA or SBA) (0 or 500  $\mu\text{M}$ ) in 50 mM HEPES buffer (pH 7.2, 0.2 mM TFA). For in RBCs (sample 4-6); A solution of probe **1** (200  $\mu\text{M}$ ) and inhibitors (0 or 1 mM) in 2 mL HBS buffer (20 mM HEPES, 107 mM NaCl, 6 mM KCl, 1.2 mM  $\text{MgSO}_4$ , 2 mM  $\text{CaCl}_2$ , 11.5 mM glucose, pH 7.4) was added to a 2.5 mL RBC suspension. After centrifugation, the supernatant was removed, and the sedimented RBCs were resuspended in 50 mM HEPES buffer (pH 7.2, 100 mM NaCl, 0.17 mM TFA, 20%  $\text{D}_2\text{O}$  (v/v)) and subjected to NMR or MRI measurements at 25°C.